Enhanced Frequency Regulation Scheme: An Online Paradigm for Dynamic Virtual Power Plant Integration

Hêmin Golpîra, Bogdan Marinescu

Enhanced Frequency Regulation Scheme: An Online Paradigm for Dynamic Virtual Power Plant Integration

Hêmin Golpîra, *Senior Member, IEEE*, Bogdan Marinescu, *Member, IEEE*

***Abstract*— This paper presents a novel measurement-based frequency regulation scheme that utilizes the contributions of inverter-based resources (IBRs). IBRs are assumed to be aggregated within dynamic virtual power plant (DVPP), conceptualized as a new entity in modern power systems that can be summoned by the system operator to provide dynamic ancillary services. While the participation of DVPPs in frequency regulation is outlined in ancillary service markets, the main objective is to distribute regulation signals among the resources within DVPPs. To achieve this, a power imbalance propagation paradigm is introduced, aiming to estimate the extent of power imbalance across the grid. Subsequently, the contribution factor is established for the purpose of evaluating the involvement of individual clusters of IBRs within the context of both primary and secondary frequency control commitments. The proposed mathematics-based approach is scalable and only needs to have access to few local measurments and exchanged power information between the adjacent neighboring areas to realize a real-time application. The effectiveness of the proposed methodologies is examined on two power grids.**

***Index Terms*-- primary frequency control, secondary frequency control, dynamic virtual power plant, power imbalance size, automatic generation control.**

NOMENCLATURE AND ABBRIVIATION

CF	Contribution factor
DVPP	Dynamic virtual power point
RES	Renewable energy source
IBR	Inverter-based resource
SG	Synchronous generator
PFC	Primary frequency control
SFC	Secondary frequency control
FRR	Frequency response reserve
AGC	Automatic generation control
ACE	Area control error
SO	System operator
COI	Center of inertia
TDS	Time domain simulation
D	Load damping factor
H_G	Inertia constant of the grid
H_{DVPP}^{i}	Inertia constant of cluster *i* located in DVPP
H_j^i	Component *j* of emulated inertia for cluster *i*
ΔP_{DVPP}^{PFC}	Power supplied to the grid by PFC
ΔP_{DVPP}^{SFC}	Power supplied to the grid by SFC
$\Delta P_{DVPP-ref}^{PFC}$	Setpoint signal for PFC
$\Delta P_{DVPP-ref}^{SFC}$	Setpoint signal for SFC
δ_i	Rotor angle
T_{m_i}	Input mechanical torque
T_{e_i}	Output electrical torque
f_i	Frequency at the CP to the grid
P_i^{Grid}	Injected power to the main grid
H_{DVPP}^{i}	Inertia constant of cluster *i* located in DVPP
H_{DVPP}	Emulated inertia constant of DVPP
$\Delta p^{cluster_i}$	Pre-fault steady-state change in the output power of cluster *i*
$\Delta P_L^{cluster_i}$	Size of power imbalance at CP of cluster *i* to the main grid
ΔP_L	Size of power imbalance
$RoCoF$	Rate of change of frequency
ω	Angular speed
$\Delta f_{ss}^{desired}$	Desired steady-state frequency deviation
β_{DVPP}	Aggregated actual frequency response characteristic of the DVPP
r	Penetration rate of IBRs

I. INTRODUCTION

Frequency regulation mechanisms play an important role in ensuring reliable and secure operation of electric power systems. As a normal part of conducting business, vertically integrated utilities i.e., large-scale synchronous generators (SGs), had the responsibility to maintain a near real-time balance between generation and load. Following deregulation in the power industry, the responsibility for frequency regulation has been redefined as an ancillary service, which is performed by parties that generate, control, and transmit electricity in support of the basic services of energy supply and power delivery [1-3]. Transition towards renewable energy sources (RESs), nevertheless, imposes that regulatory services in future power systems should be shouldered by a combination of SGs and inverter-based resources (IBRs).

Several investigations have been reported in recent years, pertaining to the application of IBRs in frequency regulation. The research conducted so far in the field can be broadly categorized into two groups: 1) model-oriented approaches and 2) model-free-based approaches. Model-oriented methods primarily focus on studying the participation of a limited

This work has received funding from the European Union's Horizon 2020 research and innovation programme under grant agreement No. 883985 (POSYTYF - POwering SYstem FlexibiliTY in the Future through RES). https://posytyf-h2020.eu/.

Hêmin Golpîra is with the Power Systems Modeling & Simulation Lab., Department of Electrical and Computer Engineering, University of Kurdistan, Kurdistan, Sanandaj 66177-15175, Iran (email: hemin.golpira@uok.ac.ir).

Bogdan Marinescu is with the Ecole Centrale Nantes-LS2N-CNRS, Nantes, France (email: bogdan.marinescu@ec-nantes.fr).

number of individual IBRs [4-7], or aggregated groups of small-scale RESs envisioned within the concept of virtual power plants (VPPs) [8-11], within the context of frequency regulation. The increasing integration of RESs, however, emphasizes the significance of regulation methods that efficiently handle operational uncertainties, a capability lacking in model-oriented approaches. More precisely, model-oriented controllers present significant real-time computational obstacles. Furthermore, frequency regulation policies necessitate the development of appropriate disaggregation-based approaches for VPPs to accurately ascertain the contribution of each source in adhering to the instantaneous regulation request, an aspect that is overlooked in recent research. Other shortcomings of the recent model-oriented studies encompass overlooking the dynamic of the host grid, disregarding the interplay between VPPs and grid frequency regulation services, and omitting consideration of RESs at the transmission level.

Model-free category mainly focuses on using learning-based techniques to determine participation of IBRs in the frequency regulation service. The utilization of IBRs for frequency regulation is addressed through reinforcement learning (RL)-based approaches in [12, 13]. A two-stage deep RL-based approach is discussed in [14] for predicting the output power of sources and issuing disaggregated request balancing signals. The primary difficulty when employing RL lies in ensuring that the learned controllers are stabilizing, resulting in frequency within the system eventually reaching a stable equilibrium following disturbances. For this purpose, existing approaches often adopt soft penalties, imposing substantial costs when states deviate from predefined ranges. Nevertheless, it is crucial to treat stability as a hard constraint rather than relying on penalties, as training can only be conducted with a limited number of samples, while the controller must ensure stability across a broader set of points in the state space. Furthermore, the typical practice involves using generated trajectories to train the neural network controllers, yet the evolution of state variables over lengthy time horizons makes direct back propagation inefficient. Moreover, challenges associated with algorithmic stability, which concerns how slight variations in input data can impact the output of a machine learning-based approach, restrict the feasibility of employing RL-based methods in real-time applications.

Lyapunov function is incorporated with RL in [15] to guarantee frequency stability. However, simply thresholding the output once the constraints are reached tend to lead to very poor performances [16]. More precisely, a primary challenge associated with this method arises when the control signal generated by the control law cannot be fully executed due to input saturation, imposing constraints on the magnitude of the control input. Furthermore, this method tries to maintain the nodal frequency of buses within a desired safe region and to recover from undesired initial conditions while could not guarantee secure operation in transient period. The need for massive datasets to train on, along with the complexity of implementation, are other important drawbacks. For more on VPP and IBRs in the context of ancillary services see [17, 18].

This paper addresses the aforementioned drawbacks by proposing a mathematical-based framework that offers frequency regulation for the power grid through appropriately dispatching the resources within a dynamic VPP (DVPP). The DVPP, which was initially conceptualized in the POSYTYF project [19, 20], is assumed to comprise a diverse range of resources, including conventional SGs and IBRs across different power levels and time scales. The proposed model-free based method relies on the fundamental mathematical equations governing power systems to generate reference balancing signals for the resources within a DVPP through primary frequency control (PFC) and secondary frequency control (SFC) loops.

To achieve the aforementioned objectives, a measurement-based approach is proposed to determine the power imbalance size at the connecting point (CP) of the resources within the DVPP to the main grid. The participation of resources within the DVPP in meeting the established frequency response reserve (FRR) is subsequently calculated based on the RoCoF and steady-state frequency deviation. The next step involves adjusting the reference power of each resource based on the steady-state frequency deviation through SFC. Finally, an algorithm is proposed for real-time updating of the disaggregated reference balancing signals in response to changing operating points. Therefore, the main contributions of this paper are as follows:

- Introducing the *power imbalance propagation paradigm*, a measurement-based approach to mathematically model the propagation of power imbalance in the grid.
- Proposing a mathematical-based approach to allocate PFC and SFC between the IBRs within a DVPP and adjust the setpoints based on real-time measurements. It can finely dispatch the resources, ensuring secure operation by maintaining the frequency dynamics, including the rate of change of frequency (RoCoF) and steady-state deviation, within a safe range. The approach is scalable and requires access to a limited number of local measurements and exchanged power data within contiguous neighboring areas, in order to facilitate the execution of a real-time application.

II. Proposed Frequency Regulation Methodology

A. Problem Definition

Consider a power system which is subjected to a physical disturbance, causing power imbalance in the system. The system operator (SO) is going to regulate the frequency by utilizing the control loops of both SGs and DVPPs, including PFC and SFC loops, as schematically represented in Fig. 1. The model in Fig. 1 is based on the notation from [21], where it is developed as a function of IBRs penetration level denoted as "*r*". To maintain a consistent 1 pu system load, the power rating of the aggregated model of SGs in the figure decreases by (1-*r*). It is noteworthy that the simplified model in Fig. 1 is solely for analysis purposes, and all simulations use a 6th-order generator model with turbine-governing systems for SGs, whereas dynamic models are applied to IBRs.

With reference to the notation in Fig. 1, one could describe the distinct participation of DVPP in both PFC and SFC as

$$\Delta P_{DVPP} = \Delta P_{DVPP}^{PFC} + \Delta P_{DVPP}^{SFC} \quad (1a)$$

and

$$\Delta P_{DVPP-ref} = \Delta P_{DVPP-ref}^{PFC} + \Delta P_{DVPP-ref}^{SFC} \quad (1b)$$

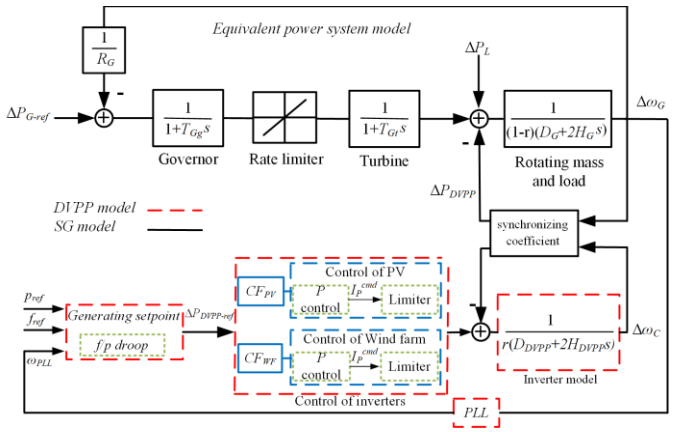

Fig. 1. Block diagram representation of frequency regulation service using SGs and DVPPs. The red blocks constitute the dynamics of the DVPP. High-order non-linear models are used in simulations and simplified models are used for analysis; CF stands for contribution factor.

where ΔP_{DVPP}^{PFC}, ΔP_{DVPP}^{SFC}, $\Delta P_{DVPP-ref}^{PFC}$, and $\Delta P_{DVPP-ref}^{SFC}$ represent the power supplied to the grid by PFC and SFC, and the setpoint signals associated with PFC and SFC, respectively.

It is important to highlight that the distinct functionalities of PFC and SFC imply that during PFC, only the terms associated with it on the right-hand side of (1) have non-zero values, while both terms remain non-zero during SFC.

PFC: The PFC is responsible for contributing to arresting frequency deviations through the provision of frequency response. Conventionally, the frequency response is defined as the sum of the inertial response, natural load response, and governor response of SGs to frequency deviation, as equivalently illustrated by H_G, D_G and R_G in Fig. 1. The commonly employed strategy for utilizing IBRs to provide PFC involves configuring them to mimic SGs, employing emulated inertial response (H_{DVPP}), emulated load response (D_{DVPP}), and *f*/*p* droop control, as illustrated in Fig. 1. However, conventional PFC mechanisms in SGs operate as autonomous loops that don't rely on external inputs to be triggered, whereas inverters are solid-state electronic devices capable of tracking power setpoints. Hence, IBRs within DVPP have the capability to rapidly respond to control signal, denoted as $\Delta P_{DVPP-ref}^{PFC}$ in (1b), promising the implementation of real-time approaches for PFC. This suggests that it is feasible to implement alternative control laws to ensure the stability of an IBR-integrated power system, surpassing a linear droop response, as proposed in other studies such as [5, 15, 22]. This possibility is investigated in this paper, which introduces a new control law, i.e., $u(\omega_{\text{pll}})$, as a replacement for the current linear *f*/*p* control law.

The SO conducts contingency analysis within specified time intervals, ranging from a few minutes to several hours, with the aim of communicating the permissible frequency and the minimum necessary quantity of FRR, in terms of MW, to the ancillary service market [23]. From the SO's point of view, DVPP is responsible for providing a fraction of FRR, denoted as ΔP_{DVPP}^{PFC}, specified based on the ancillary service market settlement. From DVPP owner's point of view, however, the resources within their territory should be dispatched appropriately to fulfil ΔP_{DVPP}^{PFC} requirement. To achieve this, ΔP_{DVPP}^{PFC} should be represented based on the emulated frequency response characteristics. Furthermore, DVPP's contribution to inertial response plays a pivotal role in the allocation of resources within DVPP. The contribution of each cluster of IBRs within the DVPP in achieving aggregated frequency response characteristics or inertia constant determines setpoint signals for each resource.

SFC: Once the PFC has arrested and stabilized frequency decline following a disturbance, SFC comes into play to restore the frequency to its nominal value using automatic generation control (AGC) system. The AGC system utilizes system frequency and net actual interchange deviations to determine the area control error (ACE) signal, which indicates whether a system is in balance or requires adjustments to generation resources. The AGC system sends real-time reference signal $\Delta P_{DVPP-ref}^{SFC}$ that prompts the DVPP to perform SFC and counteract the ACE. Again, from DVPP owner's point of view, the reference signal needs to be disaggregated among the resources within the DVPP.

B. Definitions and Hypothesis

This paper examines various hypotheses and definitions to formulate the proposed approach for frequency regulation. These encompass:

1- While a VPP exclusively handles the power injection and integration of individual RES generators into the market, the DVPP concept facilitates the integration of RES generators into the electrical grid by leveraging their collective flexibility. This involves swiftly adjusting output for frequency control, internally managing fluctuations, and marketing their combined generation output in the wholesale market. Compared to the conventional VPP, the DVPP concept will jointly address:
   - *Static power dispatch* suggests that the DVPP has the capability to manage the dispatch of all IBRs functioning in grid-forming mode, ensuring optimal operation;
   - *Dynamic power control* establishes dynamic regulation for each IBR, as well as for the DVPP, ensuring participation in grid ancillary services.

2- The DVPP is essentially defined as a group of generating units without specific criteria for its formation.

3- The DVPP includes non-dispatchable RESs operating in grid-following mode, and dispatchable ones functioning in grid-forming mode, realized using the proposed control laws. Nonetheless, the DVPP appears to the grid as a cohesive, dispatchable, and fully manageable energy source that can be fine-tuned to support ancillary services, as shown in Fig. 1. The RESs employed in this paper consist of photovoltaics (PVs) and wind generation.

4- The DVPP transmits PFC regulation instructions to IBRs every second in response to frequency fluctuations. To fully implement the SFC loop within the DVPP, it transmits SFC regulation instructions to IBRs at two distinct time intervals. The first action operates on a timescale of 4 to 5 minutes, ensuring optimal production levels of IBRs within the DVPP. The second component involves an internal power redispatch mechanism,

operating at an intermediate time-scale, approximately 4 seconds, and is the focus of this paper [24]. These update periods account for the delay linked to transmitting instructions through cellular wireless communications.

5- The DVPP does not take into account dispatchable loads.

C. Proposed method structure

The proposed frequency regulation framework consists of three main modules: (1) estimating the power imbalance size in the CP of resources to the main grid, called *power imbalance propagation paradigm*; (2) generating PFC and AGC reference balancing signals and disaggregating the signals between the resources within DVPP; and (3) real-time re-adjusting of the setpoint signals. Fig. 2 illustrates a schematic representation of the proposed frequency regulation, with emphasis on the key modules of interest highlighted in orange, providing a breakdown of the input and output signals for each module.

D. Power Imbalance Propagation Paradigm

Let to consider a power grid consisting *n* cluster of IBRs connected to the main grid at different voltage levels, as shown in Fig. 3, creating a DVPP structure. It is assumed that clusters 1, 2, …, *m* are at the distribution level, connected to the main grid via transformers T_1,…, T_m, and clusters *m*+1, …, *n* are directly connected to the transmission level. The occurred power imbalance in the system, denoted as ΔP_L, may be manifested at the CP of cluster *i*, connected to the grid either through transformer T_i or directly in Fig. 3, to the grid with a magnitude of $\Delta P_L^{cluster_i}$. The preliminary aim is to derive a relationship that can be used to calculate $\Delta P_L^{cluster_i}$ based on a few locally measurable quantities.

The rationale behind developing a framework for power imbalance propagation is rooted in the concept of local frequency estimation in modern power systems. This suggests that frequency is no longer considered a universal property of the grid and can vary from one bus to another [25-27]. Accordingly, one can express the local emulated motion of the under-study cluster using the swing equation of the form [28]

$$2H_{DVPP}^{i}\frac{d^2\delta_i}{dt^2} = \underbrace{T_{m_i}(t) - T_{e_i}(t)}_{\Delta P_L^{cluster_i}} \tag{2}$$

where $\delta_i, H_{DVPP}^{i}, T_{m_i}$ and T_{e_i} express the emulated quantities of rotor angle, inertia constant, input mechanical torque, and output electrical torque, respectively, for cluster *i*. Furthermore, $\Delta P_L^{cluster_i}$ refers to the size of power imbalance at CP of cluster *i* to the main grid.

By reorganizing the terms in (2) based on the defined expression for RoCoF as $RoCoF = \frac{d(\Delta\omega)}{dt}$, one obtains

$$2H_{DVPP}^{i} \times RoCoF^{i} = \Delta P_L^{cluster_i} \tag{3}$$

Since (3) is derived based on the concept of a virtual SG for cluster *i*, the concepts of frequency and RoCoF are defined as the primary and secondary derivative of the measured voltage phase angle, respectively. Hence, by calculating the contribution of cluster *i* to the equivalent inertia constant of the grid, denoted as H_{DVPP}^{i}, one could estimate $\Delta P_L^{cluster_i}$.

To calculate H_{DVPP}^{i}, let us define the injected power of cluster *i*, operated in the grid-forming mode, to the main grid as P_i^{Grid}. By applying $f_i - P_i^{Grid}$ data to the Prony analysis, one obtains

$$\frac{f_i}{P_i^{Grid}} = \sum_{j=1}^{K}\frac{a_j}{s+c_j} = \sum_{j=1}^{K}\frac{1}{2H_j^i s + D_j^i} \tag{4}$$

where f_i, P_i^{Grid}, H_j^i and D_j^i are frequency at the CP to the grid, injected power to the main grid, components of emulated inertia constant for cluster *i* as seen from the grid, and components of emulated damping factor for cluster *i* as seen from the grid, respectively.

Eq. (4) reveals that *K* equivalent SGs with characteristics represented by H_j^i can emulate the aggregated dynamic behavior of IBRs in cluster *i*, as viewed from the perspective of the main grid. Since these equivalent SGs are assumed to be located on the same bus as the under-studied cluster of IBRs, they exhibit complete coherence. Consequently, the emulated inertia constant of the cluster can be represented by the equivalent inertia for a group of *K* coherent SGs, namely

$$H_{DVPP}^{i} = \sum_{j=1}^{K} H_j^i \tag{5}$$

It is essential to emphasize that the analytical equation in (5) is based on locally measured quantities instead of relying on mechanical momentum, making it readily applicable to either SGs or clusters of IBRs.

Equations (3) through (5) could be interpreted as a fault propagation paradigm which could be utilized to estimate the size of power imbalance throughout the grid. Although (3) appears to decouple the dynamics of cluster *i* from the rest of the grid, the impact of the grid and disturbances is actually manifested in (4), (5), and local RoCoF measurements.

The subsequent step involves allocating the balancing power associated with PFC and SFC to the individual resources within the DVPP.

E. Frequency Regulation Framework

1) PFC

Allocating PFC commitment between the resources within the DVPP should be approached from two distinct perspectives: 1) a dynamic point of view which determines the supplementary contribution of DVPP in inertial response of the system and 2) a steady-state point of view which determines supplementary contribution of DVPP in frequency response characteristic of the system.

Dynamic point of view: The RoCoF at the center of inertia (COI) of the SG-based power grid, denoted as $RoCoF_{COI}$, after the occurrence of the power imbalance ΔP_L can be computed using (3) as

$$RoCoF_{COI} = \frac{\Delta P_L}{2H_G} \tag{6}$$

where H_G is the equivalent grid inertia constant.

Given the involvement of DVPP in the PFC, one could express the $RoCoF_{COI}$ based on the equivalent inertia $H_G + H_{DVPP}$, as

$$RoCoF_{COI} = \frac{\Delta P_L}{2(H_G + H_{DVPP})} \tag{7}$$

Secure operation of the system requires that the RoCoF following the occurrence of the power imbalance should remain within a pre-specified range, as defined in the grid codes, namely

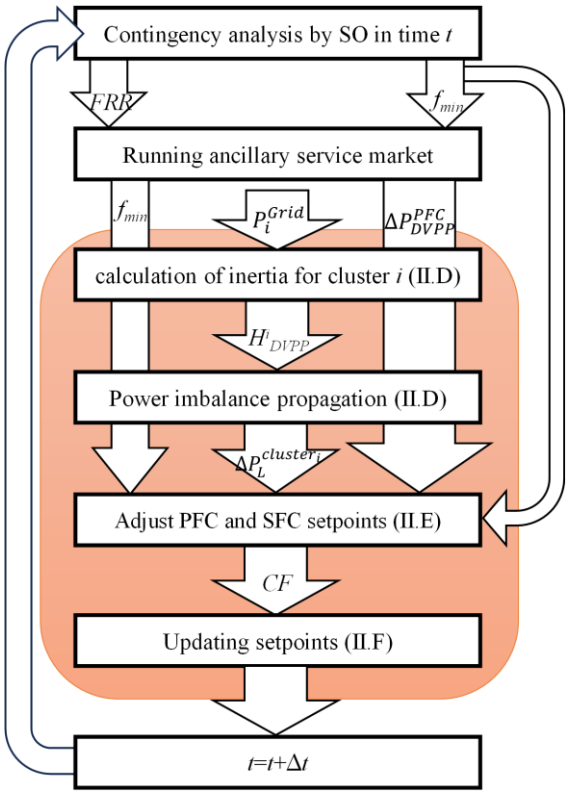

Fig. 2. A general description of the proposed frequency regulation scheme.

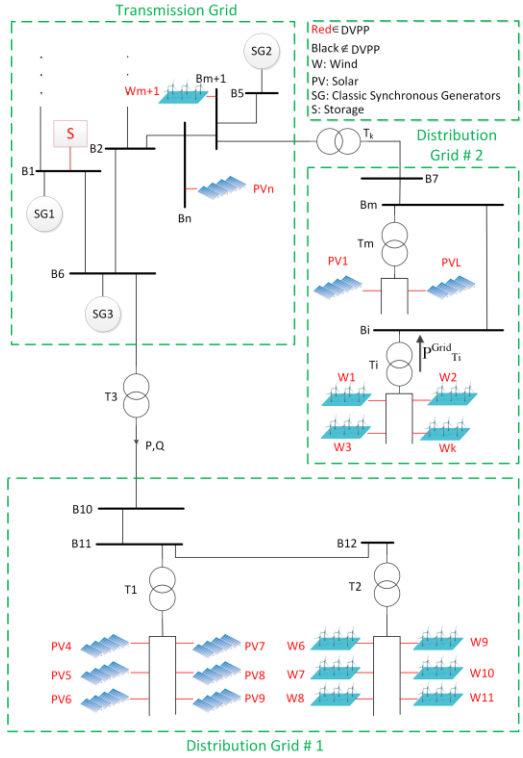

Fig. 3. Power system including DVPP.

$$\frac{\Delta P_L}{2(H_G + H_{DVPP})} \leq RoCoF^{des} \tag{8}$$

where $RoCoF^{des}$ is the desired RoCoF.

Re-arranging the term in (8) yields to

$$H_{DVPP} \geq \frac{\Delta P_L}{2RoCoF^{des}} - H_G \tag{9}$$

Indeed, the right-hand side of (9) specifies the minimum contribution of DVPP in the system to ensure secure operation, adhering to the RoCoF requirements. Here, it should be noted that IBRs operating in a grid-forming mode may enhance the system's overall inertia using the virtual SG concept, making it feasible to adjust the inertia level for a specific system in real-time, as addressed in research works such as [29, 30]. Consequently, equation (9) gains practical significance.

To calculate the contribution of each cluster of resources within the DVPP to realize H_{DVPP} (9), consider the i^{th} cluster in Fig. 3. Secure operation of the grid imposes that, except for the RoCoF at COI, the RoCoF at the CP of cluster i to the main grid should also adhere to the specified $RoCoF^{des}$. More precisely, one can express the constraint on the local RoCoF at the CP of cluster i to the grid based on (3) and (6) as

$$\frac{\Delta P_L^{cluster_i}}{2H^i_{DVPP}} \leq RoCoF^{des} \rightarrow H^i_{DVPP} \geq \frac{\Delta P_L^{cluster_i}}{2RoCoF^{des}} \tag{10}$$

The right-hand side of (10) specifies the minimum required inertia for cluster i to comply with the grid codes regarding RoCoF.

By calculating minimum H^i from (10), one can determine the contribution factor (CF) of cluster i from a dynamic perspective, denoted as CF_i^D, as

$$CF_i^D = \frac{H^i_{DVPP}}{H_{DVPP}} \tag{11}$$

While (11) is used to calculate n-1 CFs related to the associated clusters, the n^{th} CF^D is calculated in a way that satisfies the overall H_{DVPP}. To achieve this, one can write

$$CF_n^D = 1 - \frac{\sum_{i=1}^{n-1} H^i_{DVPP}}{H_{DVPP}} \tag{12}$$

It is noteworthy that although equations (11) and (12) should produce identical results, measurement errors in RoCoF and simplifications in calculations can introduce some differences. This implies that the n^{th} cluster is designated as the slack cluster in (12) to compensate for the balancing power required to precisely meet H_{DVPP}.

The physical interpretation of (11) and (12) holds true only when either the RoCoF at COI or the CP of clusters exceeds the desired value; otherwise, the CF^D is regarded as zero.

Steady-state point of view: The steady-state frequency deviation following occurrence of the power imbalance ΔP_L can be calculated by [31]

$$\Delta f_{ss} = \frac{\Delta P_L}{\beta_G} \tag{13}$$

where

$$\beta_G = \frac{1}{R_G} + D_G \tag{14}$$

In (13) and (14) $\Delta f_{ss}, \beta_G, R_G$ and D_G are steady-state frequency deviation, frequency response characteristic of the grid, droop characteristic of the gird, and load damping of the grid, respectively.

On the other hand, the steady-state frequency deviation in response to the contribution of DVPP in PFC can be explained using the equivalent frequency response characteristics i.e., $\beta_G + \beta_{DVPP}$, based on (13), as

$$\Delta f_{ss}^{desired} = \frac{\Delta P_L}{\beta_G + \beta_{DVPP}} \tag{15}$$

and

$$\beta_{DVPP} = \frac{r}{R_{DVPP}} + rD_{DVPP} \tag{16}$$

where $r, \Delta f_{ss}^{desired}$ and β_{DVPP} are participation factors of DVPP for the under-study operating point, desired steady-state frequency deviation after provision of FRR, and aggregated actual frequency response characteristic of the DVPP, respectively.

While the aim is to calculate β_{DVPP} in (15), $\Delta f_{ss}^{desired}$ is also an unknown parameter. However, $\Delta f_{ss}^{desired}$ can be calculated from the SO's point of view where the DVPP can be represented by the FRR power ΔP_{DVPP}^{PFC}. More precisely, $\Delta f_{ss}^{desired}$ can be calculated as

$$\Delta f_{ss}^{desired} = \frac{\Delta P_L - \Delta P_{DVPP}^{PFC}}{\beta_G} \tag{17}$$

By having $\Delta f_{ss}^{desired}$ from (17), one can calculate β_{DVPP} for the overall DVPP, based on (15), as

$$\beta_{DVPP} = \frac{\Delta P_L}{\Delta f_{ss}^{desired}} - \beta_G \tag{18}$$

To calculate the contribution of each cluster of sources within the DVPP to realize β_{DVPP} (18), again consider the i^{th} cluster in Fig. 3. Secure operation of the grid imposes that the steady-state frequency deviation at the CP of the clusters to the main grid should be the same as that of $\Delta f_{ss}^{desired}$ in (17). More precisely, one can express the local steady-state frequency deviation in the CP of cluster *i* to the grid based on (3) and (13) as

$$\Delta f_{ss}^{i} = \frac{\Delta P_L^{cluster_i}}{\beta_{DVPP}^{cluster_i}} \xrightarrow{\Delta f_{ss}^{i} = \Delta f_{ss}^{desired}} \beta_{DVPP}^{cluster_i} = \frac{\Delta P_L^{cluster_i}}{\Delta f_{ss}^{desired}} \tag{19}$$

where Δf_{ss}^{i} and $\beta_{DVPP}^{cluster_i}$ are steady-state frequency deviation at the CP of cluster *i* to the main grid and frequency response characteristic of cluster *i*, respectively.

By calculating $\beta_{DVPP}^{cluster_i}$ from (19), one could calculate the CF of cluster *i* from a steady-state perspective, denoted as CF_i^{ss}, as

$$CF_i^{ss} = \frac{\beta_{DVPP}^{cluster_i}}{\beta_{DVPP}} \tag{20}$$

Again, by considering the n^{th} cluster as slack cluster, one can write

$$CF_n^{ss} = 1 - \frac{\sum_{i=1}^{n-1} \beta_{DVPP}^{cluster_i}}{\beta_{DVPP}} \tag{21}$$

The final CF of each cluster, which satisfies both the dynamic and steady-state aspects, can be defined as

$$CF_i = \max\{CF_i^{ss}, CF_i^{D}\} \tag{22}$$

With the CF for cluster *i* determined, the contribution of the cluster in realizing FRR power ΔP_{DVPP}^{PFC}, represented by $\Delta P_{DVPP}^{PFC_i}$, which aligns with the associated reference signal denoted as $\Delta P_{DVPP-ref}^{PFC_i}$, is defined as

$$\Delta P_{DVPP-ref}^{PFC_i} \cong \Delta P_{DVPP}^{PFC_i} = CF_i \times \Delta P_{DVPP}^{PFC} \tag{23}$$

2) AGC

PFC stabilizes frequency at a value lower than the nominal one. Therefore, the SO needs to provide an auxiliary reference signal to the DVPP in order to restore frequency to the nominal value. To achieve this, the difference between ΔP_L and ΔP_{DVPP}^{PFC} should be compensated by the $\Delta P_{DVPP-ref}^{SFC}$ in Fig. 1. However, the primary concern is how to allocate the reference signal among the sources within the DVPP.

To disaggregate the reference signal, let's define the overall ACE as [32]

$$ACE = AIP - SIP - B(f_a - f_s) \tag{24}$$

where AIP, SIP, B, f_a, and f_s are actual interchanged power, scheduled interchanged power, frequency bias, actual frequency, and nominal frequency, respectively.

As the steady-state frequency is common throughout an interconnection following provision of the FRR, one can write ACE for cluster *i*, based on (24), as

$$ACE_i = AIP_i - SIP_i - B(f_i - f_s) \tag{25}$$

As PFC and AGC affect system dynamics via emulated turbine-governor behavior but using different inputs, the reference signal for cluster *i*, can be calculated using the same procedure as in (20), namely

$$\Delta P_{DVPP-ref}^{SFC_i} = \frac{ACE_i}{ACE}(\Delta P_L - \Delta P_{DVPP}^{PFC}) \tag{26}$$

where $\Delta P_{DVPP-ref}^{SFC_i}$ denotes SFC reference signal for cluster *i*.

F. Real-time re-adjusting of the setpoints

1) PFC

Now, let's assume that in response to changing the operating point or the size of power imbalance, the output power of sources changes. The main problem of interest is to update $\Delta P_{DVPP-ref}^{PFC_i}$ in (23) based on a few measured quantities from the grid to meet the new PFC requirements, namely

$$\Delta P_{DVPP-ref}^{PFC_{i,new}} = \underbrace{(CF_i + \Delta CF_i)}_{CF_i^{new}} \times \Delta P_{DVPP}^{PFC} \tag{27}$$

Eq. (27) illustrates that in order to obtain the updated reference signal, the new CF needs to be calculated. First, let to consider $CF_i = CF_i^{ss}$ in (22). Considering the long-term nature of the frequency dynamics in frequency regulation studies, one could express the deviation of CF_i based on the Taylor expansion form of (20) as

$$\begin{aligned} &CF_i + \Delta CF_i \\ &= \frac{\beta_{DVPP}^{cluster_i}}{\beta_{DVPP}} + \frac{1}{\beta_{DVPP}} \frac{\partial \beta_{DVPP}^{cluster_i}}{\partial \Delta p^{cluster_i}} \Delta p^{cluster_i} \\ &+ \frac{\frac{\partial \beta_{DVPP}^{cluster_i}}{\partial \Delta P_L} \beta_{DVPP} - \frac{\partial \beta_{DVPP}}{\partial \Delta P_L} \beta_{DVPP}^{cluster_i}}{{\beta_{DVPP}}^2} \Delta(\Delta P_L) \end{aligned} \tag{28}$$

where $\Delta p^{cluster_i}$ refers to the pre-fault steady-state change in the output power of cluster *i* in response to a changing operating point.

According to (19), the second term on the right-hand side of (28) could be re-written as

$$\frac{1}{\beta_{DVPP}} \frac{\partial \left(\frac{\Delta P_L^{cluster_i}}{\Delta f_{ss}^{desired}}\right)}{\partial \Delta p^{cluster_i}} \Delta p^{cluster_i} = \frac{1}{\beta_{DVPP}} \frac{\Delta p^{cluster_i}}{\Delta f_{ss}^{desired}} \tag{29}$$

Following the same notation as in (29), the third term on the right-hand side of (28) could be represented by

$$\begin{aligned} &\frac{\frac{\partial \beta_{DVPP}^{cluster_i}}{\partial \Delta P_L} \beta_{DVPP} - \frac{\partial \beta_{DVPP}}{\partial \Delta P_L} \beta_{DVPP}^{cluster_i}}{{\beta_{DVPP}}^2} \Delta(\Delta P_L) \\ &= \frac{\partial \left(\frac{\Delta P_L^{cluster_i}}{\Delta f_{ss}^{desired}}\right) \beta_{DVPP} - \partial \left(\frac{\Delta P_L}{\Delta f_{ss}^{desired}} - \beta_G\right) \beta_{DVPP}^{cluster_i}}{\frac{\partial \Delta P_L}{{\beta_{DVPP}}^2}} \Delta(\Delta P_L) \end{aligned} \tag{30}$$

To further simplify (30), a relationship between $\Delta P_L^{cluster_i}$ and ΔP_L should be derived. For this purpose, dividing (19) by (15) results in

$$\frac{\Delta P_L^{cluster_i}}{\beta_{DVPP}^{cluster_i}} = \frac{\Delta P_L}{\beta_G + \beta_{DVPP}} \rightarrow \Delta P_L^{cluster_i} = \frac{\beta_{DVPP}^{cluster_i}}{\beta_G + \beta_{DVPP}} \Delta P_L \tag{31}$$

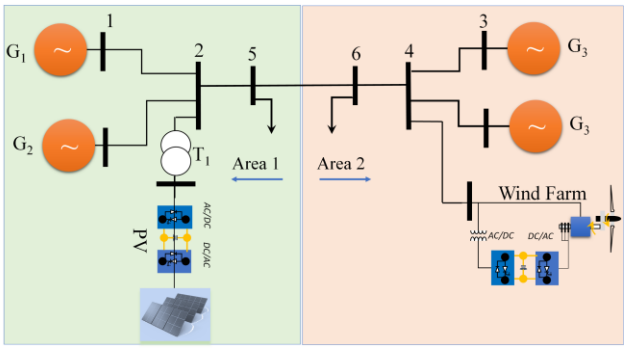

Fig. 4. Modified two-area test system.

Substituting (31) into (30) using the definition of (15) gives

$$\frac{\partial \beta_{DVPP}^{cluster_i}}{\partial \Delta P_L}\Delta(\Delta P_L) = \left(\frac{\frac{\beta_{DVPP}^{cluster_i}}{\beta_G+\beta_{DVPP}}\Delta f_{ss}^{desired} - \frac{\Delta P_L^{cluster_i}}{\beta_G+\beta_{DVPP}}}{\left(\Delta f_{ss}^{desired}\right)^2}\right)\beta_{DVPP} = \frac{}{{\beta_{DVPP}}^2}\Delta(\Delta P_L) - \frac{\frac{\beta_{DVPP}^{cluster_i}}{\Delta f_{ss}^{desired}}}{{\beta_{DVPP}}^2}\Delta(\Delta P_L) \quad (32)$$

By replacing (29) and (32) into (28) and rearranging the terms, the final equation takes the form

$$\Delta CF_i = \frac{1}{\beta_{DVPP}}\frac{\Delta p^{cluster_i}}{\Delta f_{ss}^{desired}} - \frac{\beta_{DVPP}^{cluster_i}\beta_G\Delta f_{ss}^{desired} + \beta_{DVPP}\Delta P_L^{cluster_i}}{(\beta_G+\beta_{DVPP}).\left(\Delta f_{ss}^{desired}\right)^2.{\beta_{DVPP}}^2}\Delta(\Delta P_L) \quad (33)$$

Now, let to consider $CF_i = CF_i^D$ in (22). By following the same procedure as in (33), one can write

$$\Delta CF_i = \frac{H_{DVPP}^{cluster_i}\Delta RoCoF^{cluster_i}(1-\Delta(\Delta P_L))}{\Delta P_L} \quad (34)$$

The new contribution factor CF_i^{new} can be computed by replacing ΔCF_i, obtained from (33) or (34) based on the selection made in (22), into (27). Indeed, (33) and (34) demonstrate that the PFC setpoint of the sources can be readjusted by simply monitoring changes in the output power of the sources within the DVPP, the disturbance size, and the local RoCoFs.

2) AGC

In another effort to fully achieve an online frequency regulation scheme, the SO is going to update the reference signal $\Delta P_{DVPP-ref}^{SFC_I}$ in (26) in response to changing ACE. Following the same procedure as in (27)-(34), one could write

$$\Delta P_{DVPP-ref}^{SFC_{i,new}} = \Delta P_{DVPP-ref}^{SFC_i} + \Delta\left(\Delta P_{DVPP-ref}^{SFC_i}\right) \quad (35)$$

Applying Taylor expansion to (26) results in

$$\Delta\left(\Delta P_{DVPP-ref}^{SFC_i}\right) = \frac{\partial \Delta P_{DVPP-ref}^{SFC_i}}{\partial ACE_i}\Delta(ACE_i) + \frac{\partial \Delta P_{DVPP-ref}^{SFC_i}}{\partial ACE}\Delta(ACE) = \frac{\left(\Delta P_L - \Delta P_{DVPP}^{PFC}\right)}{ACE}\Delta(ACE_i) - \frac{ACE_i \times \left(\Delta P_L - \Delta P_{DVPP}^{PFC}\right)}{ACE^2}\Delta(ACE) \quad (36)$$

The updated SFC reference signal for cluster i can be calculated by substituting (36) in (35).

G. Scalability

The realization of (33) through (36) in an online application requires measuring two sets of measurements, including 1) local dynamics of ACE_i, $RoCoF^{cluster_i}$ and variations in the output power of resources ($\Delta P_L^{cluster_i}$), and 2) a global dynamic ACE. As the dynamic grid model in frequency regulation studies is divided into coherent subsystems connected by a limited number of tie-lines, the global dynamic ACE signal and its variations can be easily measured by monitoring the exchanged power through these tie-lines. Hence, it becomes evident that the proposed framework can alleviate the computational burden by compressing the required measurements in the tie-lines and a few local measurements, which demonstrate scalability of the method.

H. Technical Considerations and Limitations

Before validating the proposed control laws through time domain simulation (TDS) results, it is essential to address certain technical aspects concerning the involvement of IBRs at the distribution level in ancillary services. Given that the DVPP, as a new entity, actively engages in the ancillary service market, it focuses solely on constraints linked to its generation resources, overlooking technical constraints imposed by the distributed network. These include limitations such as line and transformer thermal thresholds, over/under voltages in both steady-state and dynamic scenarios, and the erroneous activation of protection mechanisms. This query could be addressed by incorporating the distribution system operator (DSO) into the contingency analysis conducted by the SO. To be more precise, the approved contract between the SO and DVPP must receive the DSO approval before implementation. The method presented in this paper only revolves around distributing regulation services among clusters of IBRs within DVPP. The exploration of the potential and challenges associated with DSO-SO coordination is discussed in [33].

III. Simulation and Results

Exploratory studies are conducted to assess the effectiveness of the proposed formulations using two test systems: 1) a two-area power system, and 2) a large-scale New York-New England (NYNE) test system.

A. Two-Area test system

Figure 4 shows a modified single-line diagram of the two-area test system, adapted from [34]. The system consists of four SGs and a DVPP, realized using an array of PVs in the distribution level, connected to the main grid via transformer T_1, and a wind farm in transmission level in area 2. The level of RESs penetration, denoted as r in Fig. 1, is established at 35%. Among these, 65% operate in grid-forming mode as dispatchable sources, while 35% operate in grid-following mode as non-dispatchable sources. The IBRs within the DVPP functioning in grid-forming mode are presumed to supply regulatory power, encompassing FRR and AGC. A regulation reserve for wind farms and solar panels is ensured by considering a deloading primary control. This provides active power margin in the maximum power point tracking (MPPT) algorithm, usually considered to be 10% of the nominal power of the generator [24, 35].

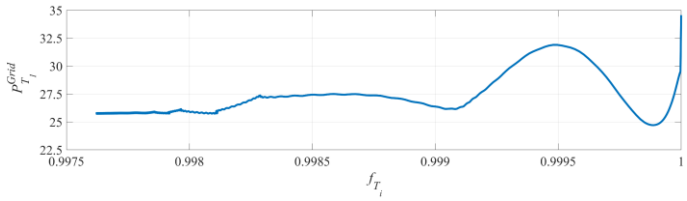

Fig. 5. Injected power of cluster of interest to the main grid.

To evaluate the effectiveness of the proposed method, a 5% load disturbance representing a power surge of 58.4 MW is applied at bus 5 in area 1. It is assumed that according to the PFC market settlement, the DVPP is responsible for providing 20 MW FRR i.e., $\Delta P_{DVPP}^{PFC} = 20$.

The steady-state frequency deviation in response to the applied disturbance can be calculated based on (13) as

$$\Delta f_{ss} = \frac{0.05}{0.5653} = 0.088 \tag{37}$$

The provision of the FRR by the DVPP imposes, as per (17), a steady-state frequency deviation of

$$\Delta f_{ss}^{desired} = \frac{0.05 - 0.0171}{0.5653} = 0.0582 \tag{38}$$

By substituting the steady-state frequency deviation (38) into (18), one has

$$\beta_{DVPP} = \frac{0.05}{0.0582} - 0.5653 = 0.294 \tag{39}$$

Now, let to calculate the *CFs* for the sources within the DVPP. For this purpose, the injected power of the PV arrays through T_1 to the main grid versus measured frequency at T_1, as shown in Fig. 5, is applied to the Prony analysis. Decomposing the resulting signal, as illustrated in Figure 5, using (4), leads to

$$\frac{f_1}{P_1^{Grid}} = \frac{1}{0.22s + 0.04} + \frac{1}{0.11s + 0.013} + \frac{1}{0.073s + 0.009} + \frac{1}{0.011s + 0.004} \tag{40}$$

By substituting the constitute components of the signal in (40) into (5), one could write the emulated inertia constant of the PV arrays, as seen from the gird, as

$$H_{DVPP}^{1} = 0.22 + 0.11 + 0.073 + 0.011 = 0.41422 \tag{41a}$$

Furthermore, one can write for cluster 2 as:

$$H_{DVPP}^{2} = 0.1373 \tag{41b}$$

Taking into account the measured RoCoF of 0.013 pu/sec in the CP of the PV arrays to the main grid and utilizing the power imbalance propagation paradigm (3)-(5), the local size of the power imbalance can be calculated as

$$\Delta P_L^{cluster_i} = 0.41422 \times 0.013 = 0.00538 \tag{42}$$

By having the power imbalance size (42) and the desired steady-state frequency deviation (38), $\beta_{DVPP}^{cluster_1}$ can be calculated based on (19) as

$$\beta_{DVPP}^{cluster_1} = \frac{0.00538}{0.0582} = 0.092 \tag{43}$$

Finally, the CF of the PV arrays in PFC can be calculated using (20) as follows

$$CF_1^{ss} = \frac{0.092}{0.294} = 0.31 \tag{44}$$

From a dynamic perspective, the RoCoF at the COI can be calculated using (6), as

$$RoCoF = \frac{0.05}{2(7.394)} \times 60 = 0.2\ [\frac{Hz}{s}] \tag{45}$$

TABLE I
COMPARISON OF PFC FOR THE PROPOSED METHOD AND [15]

Cluster	1	2
Proposed method	6.20	13.80
Ref. [15]	6.31	13.65

TABLE II
COMPARISON OF PFC FOR THE PROPOSED METHOD AND [15] CONSIDERING HARD CONSTARINT

Cluster	1	2
Proposed method	6	14
Ref. [15]	6	13.98

The RoCoF obtained from (45) inherently meets the target value of 0.5 Hz/s without requiring any DVPP involvement, effectively eliminating the minimum DVPP contribution needed for inertial response. Moreover, the second derivative of voltage angle multiplied by 2π at the CP of clusters 1 and 2 also falls within the acceptable range, resulting in the CF of the clusters being zero as well. Therefore, one can write for the overall CF based on (22) as

$$CF_1 = \max\{0.31, 0\} = 0.31 \tag{46}$$

Furthermore, one could write for the CF of the wind farm, based on (21), as

$$CF_2 = 1 - 0.31 = 0.69 \tag{47}$$

When calculating CF_2 using (20), a discrepancy of 1.3% is observed compared to (47), primarily due to measurement errors.

The calculation for determining the PFC setpoint signal to be assigned to cluster 1 within the DVPP can be derived using (23) in the following manner:

$$\Delta P_{DVPP-ref}^{PFC_1} = 0.31 \times 20 = 6.2 \tag{48}$$

Furthermore, one can write for cluster 2 as

$$\Delta P_{DVPP-ref}^{PFC_2} = 0.69 \times 20 = 13.8 \tag{49}$$

Now, let's compare the PFC results given in (48) and (49) with those obtained using [15]. Table I provides the comparison of the contribution of clusters 1 and 2 in providing active power for PFC.

The findings demonstrate that while the approach of [15] achieves the contracted PFC with a negligible error, the proposed method precisely fulfills the specified 20 [MW] requirement. Of greater significance, both methods achieve frequency regulation with a single control action, indicating that the primary setpoint signals produced by the control laws are effectively meeting the desired dynamics.

Now, let's explore a situation where the output power of cluster 1 is bounded to a maximum of 6 [MW]. The proposed method, once again, generates the outcomes presented in Table II using a single control action, while [15] requires three control actions to achieve convergence to the results. Reliance on only one control action, ensuring low computational burden, for the proposed method makes it attractive for practical applications. Nonetheless, the incorporation of the hard constraint into [15] poses a cut-off value to the control input, leading to discrepancies between the desired and actual frequencies after each control action. As a result, it required the control laws to generate new setpoints. When coordinating with SGs to provide PFC, these successive adjustments of the IBR setpoints lead to unnecessary governor mechanical movements, which reduces the governor's lifetime.

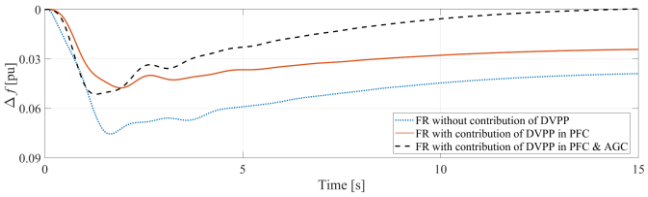

Fig. 6. Comparison of FR of the two-area test system considering contribution of DVPP in frequency regulation.

On the other hand, the AGC system should compensate for the frequency deviation of (38). To accomplish this, one can express the reference signal for the PV arrays in Fig. 4, based on (26), as

$$\Delta P_{DVPP-ref}^{SFC_1} = \frac{31}{72}(58.4 - 20) = 16.53 \quad (50)$$

Then, the reference signal for cluster 2, designated as slack, can be expressed as

$$\Delta P_{DVPP-ref}^{SFC_2} = \frac{72 - 31}{72}(58.4 - 20) = 21.87 \quad (51)$$

Upon calculating $\Delta P_{DVPP-ref}^{SFC_2}$ with the use of (26), a disparity of 0.9% is noted when compared to the value obtained from (51), mainly attributable to measurement errors.

Figure 6 compares the frequency responses (FRs) of the system with and without the contribution of the DVPP. The findings demonstrate that the PFC and AGC setpoint signals transmitted to clusters 1 and 2, as referenced in (48) via (51), are capable of arresting frequency decline and returning it to its nominal value. In this context, it is crucial to emphasize that the slight difference in frequency nadir between scenarios with only PFC and those incorporating both PFC and AGC can be attributed to the different number of IBRs required to operate in grid-forming mode to meet AGC requirements, as opposed to using PFC alone. More precisely, in response to the deloading of resources that contribute to SFC and to maintain the targeted penetration level of RESs in the system, the quantity of wind turbines has been increased, thereby accounting for this discrepancy.

Now, let to consider a situation where the output power of the sources in clusters 1 and 2 changes in response to weather changes. The new PFC setpoint signal can be calculated using both (27) and (33), specifically

$$\Delta P_{DVPP-ref}^{PFC_{1,new}} = \left(0.31 + \frac{1}{0.294}\frac{-0.0014}{0.0582}\right) \times 20 = 4.56 \quad (52)$$

Recalculating the exact setpoint signal using the same procedure as in (37)-(49) results in the new setpoint of 4.54. This means that (52) yields a result with an error of approximately 0.44%, which is promising for online applications.

Another attempt is made to calculate the new setpoint signal in response to changes in both weather conditions and the applied fault. For his purpose, ΔCF_i can be written using (33) as

$$\Delta CF_i = \frac{1}{0.294}\frac{-0.0019}{0.0582} - \frac{0.092 \times 0.5653 \times 0.0582 + 0.294 \times (-0.0019)}{(0.5653 + 0.294) \times (0.0582)^2 \times 0.294^2}(-0.01) = -0.11 - 0.096 = -0.206 \quad (53)$$

The new PFC setpoint signal reported in (54) is then calculated by substituting (53) into (27), which is well fitted to the results obtained using the same procedure as in (37)-(49), with an error of 0.31%.

$$\Delta P_{DVPP-ref}^{PFC_{1,new}} = (0.31 - 0.206) \times 20 = 2.08 \quad (54)$$

Moreover, it is expected that frequency trace for the case with the contribution of the DVPP experiences smaller frequency deviation at the nadir point compared to the trace without the DVPP. The variation in the nadir between both traces is attributed to the DVPP's contribution to the system's inertial response. To calculate this contribution, consider the derived equation in [36], as

$$H = \frac{T_n \Delta P_L}{4\Delta f_{nadir}} \quad (55)$$

where T_n and Δf_{nadir} are frequency nadir time and variation of frequency nadir, respectively.

Referring to the traces associated with frequency response with and without the contribution of DVPP in Figure 6, and utilizing equation (55), one can express the following:

$$\Delta H = \frac{2.4 \times 0.05}{4 \times 0.0386} - \frac{1.6 \times 0.05}{4 \times 0.0887} = 0.5510 \quad (56)$$

The mathematically derived inertia deviation of (56) aligns closely with the calculated inertia constant for the DVPP in (41a) and (41b). This further substantiates the accuracy of the proposed methods in this paper.

Now, let to assume that the applied disturbance in the system changes by 10 MW i.e., $\Delta P_L = 48.4$. The variation in the SFC reference signal for cluster 1 can be calculated using (36), as

$$\Delta\left(\Delta P_{DVPP-ref}^{SFC_1}\right) = \frac{(58.4 - 20)}{72}0.7 - \frac{51 \times (58.4 - 20)}{72^2} \times 15.12 = -5.324 \quad (57)$$

To enable precise compensation for the change in power imbalance within the AGC system, one can express the variation of the setpoint signal for the slack cluster as

$$\Delta\left(\Delta P_{DVPP-ref}^{SFC_2}\right) = -10 - (-5.324) = -4.676 \quad (58)$$

After conducting the calculation of $\Delta\left(\Delta P_{DVPP-ref}^{SFC_2}\right)$ using (36), a discrepancy of 1.2% is observed in comparison to the value obtained from (58).

B. NYNE test system

In another attempt, the efficiency of the proposed method is investigated on a large-scale system. Figure 7 presents a single-line diagram of the NYNE test system, illustrating the generator buses and coherent areas. The system consists of five geographical regions, 68-Bus, 16-Machine, and a DVPP comprising 5 cluster of RESs. In this representation, generators G_1 to G_{12} are equipped with a fourth-order type II power system stabilizer, tuned to provide sufficient damping [37]. It is assumed that the SGs have governor in service. Additionally, the DVPP participate in both PFC and SFC services. The realization of the DVPP is as follows

- Wind farms in transmission level in bus 8, in area 1.
- PV arrays in distribution level in bus 35, in area 2.
- Wind farms in transmission level in bus 47, in area 3
- Wind farms in transmission level in bus 42, in area 4
- Wind farm in transmission level in bus 50, in area 5

The RESs penetration level is set at 35%, with 70% functioning in grid-forming mode and 30% in grid-following mode. Of note that 15% of the nominal power of wind farms

and 10% of the nominal power of solar panels functioning in grid-forming mode are considered as an active power margin for regulation service.

To evaluate the efficiency of the proposed method on the NYNE test system, four different scenarios are considered as

- Scenario 1: Tripping of G_2 in area 1 without fault
- Scenario 2: Tripping of G_{10} in area 2 without fault
- Scenario 3: Switching on of a load at bus 7
- Scenario 4: Shedding of 24.7 pu active load in bus 18

Firstly, the size of power imbalances in the CP of the clusters to the main grid for the aforementioned scenarios is calculated using power imbalance propagation paradigm. Table III reports the size of power imbalances, which are obtained by following the same procedures as those in (39)-(42).

To further evaluate the accuracy of the results in Table III, the quantities are compared with those obtained using local dynamics estimation methods [26, 27]. The maximum errors associated with each scenario are reported in Table IV.

The per unit PFC setpoints ($\Delta P_{DVPP-ref}^{PFC_i}$), obtained through the identical methods outlined in (37) to (49), for the five cluster of sources within the DVPP, are reported in Table V. Moreover, the per unit reference signals transmitted by the AGC system to restore the frequency to its nominal value, obtained using (50) and (51), are reported in Table VI.

Figures 8-11 depict the frequency responses of the center of inertia (COI) for the scenarios. The analysis of TDS results is employed to validate the design of control-responsive outputs allocation to IBRs. In this context, the allocation of reference signals among the resources within DVPP for participation in PFC is related to stability issues, ensuring that the system remains within the permissible range for RoCoF and frequency nadir. Based on Fig. 8 and the reported results in Table VII, it is apparent that, although the RoCoF for the trace without DVPP contribution deviates from the acceptable value of 0.5 Hz/sec, the proper distribution of FRR among the IBRs guarantees operation within the allowable RoCoF range. Furthermore, Table VII compares the values of RoCoF for the traces in Figs. 8-11 with those obtained using [15], highlighting the high efficiency of the proposed method in enhancing the frequency behavior of the system. On the other hand, the TDS validates the allocation of resources to provide SFC, which is a regulatory duty rather than stability-related issue.

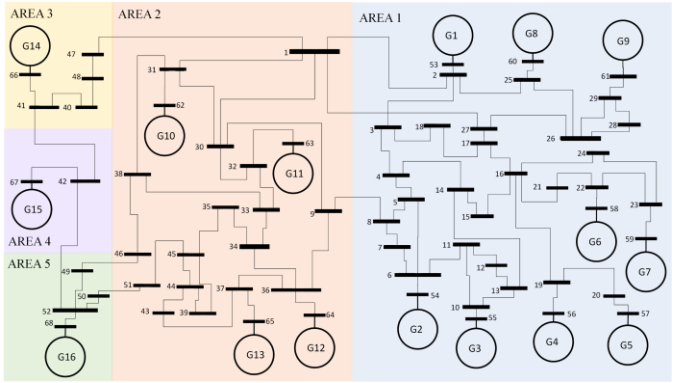

Fig. 7. NYNE test system.

In another analysis, the variation of PFC setpoint signals in response to changes in the weather and applied fault is calculated using (27) and either (32) or (33), with the specific equation selection governed by (22). The variations in these parameters, represented as percentages of the primary values on which Table V is based, are reported in Table VIII. Table IX reports the new PFC setpoint signals.

The discrepancies between the values in Table IX and the exact results obtained using the same procedures as in (37)-(49) are also documented in Table X. These findings hold promise for the practical implementation of online applications for dispatching DVPP resources and facilitating frequency regulation.

TABLE III
SIZE OF POWER IMBALANCES IN THE CP OF THE CLUSTERS TO THE MAIN GRID

#	$\Delta P_L^{cluster_1}$	$\Delta P_L^{cluster_2}$	$\Delta P_L^{cluster_3}$	$\Delta P_L^{cluster_4}$	$\Delta P_L^{cluster_5}$
1	0.00713	0.00321	0.00593	0.00538	0.00661
2	0.00215	0.00391	0.00281	0.00407	0.00112
3	0.00553	0.00641	0.00219	0.00201	0.00253
4	0.00180	0.00012	0.00222	0.00103	0.00098

TABLE IV
ACCURACY OF POWER IMBALANCE PROPAGATION PARADIGM TO ESTIMATE POWER IMBALANCE SIZE

	Maximum error	*Maximum error location*
Scenario 1	0.11%	CP_1
Scenario 2	0.16%	CP_1
Scenario 3	0.38%	CP_4
Scenario 4	0.08%	CP_3

TABLE V
PFC SETPOINT OF SOURCES IN NYNE TEST SYSTEM FOR FOUR DIFFERENT SCENARIOS

$\Delta P_{DVPP-ref}^{PFC_i}$	*Area 1*	*Area 2*	*Area 3*	*Area 4*	*Area 5*
Scenario 1	0.23	0.11	0.20	0.08	0.38
Scenario 2	0.18	0.18	0.24	0.10	0.30
Scenario 3	0.06	0.45	0.23	0.15	0.11
Scenario 4	0.22	0.13	0.31	0.16	0.18

TABLE VI
AGC REFERENCE SIGNALS IN PU

$\Delta P_{DVPP-ref}^{SFC_i}$	*Area 1*	*Area 2*	*Area 3*	*Area 4*	*Area 5*
Scenario 1	0.41	0.13	0.23	0.11	0.12
Scenario 2	0.18	0.39	0.21	0.07	0.15
Scenario 3	0.29	0.28	0.11	0.19	0.13
Scenario 4	-0.22	-0.14	-0.33	-0.21	-0.10

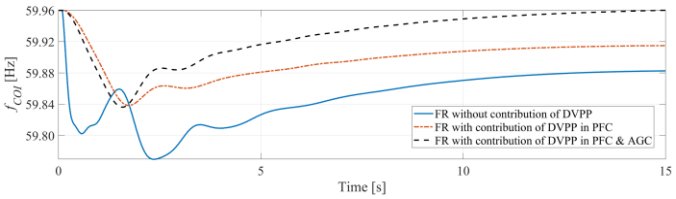

Fig. 8. Comparison of FR of the NYNE test system with and without contribution of DVPP for scenario 1.

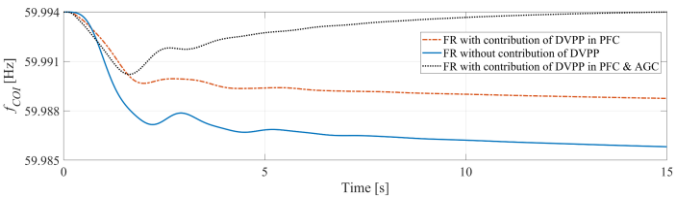

Fig. 9. Comparison of FR of the NYNE test system with and without contribution of DVPP for scenario 2.

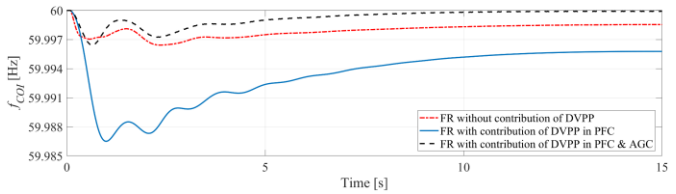

Fig. 10. Comparison of FR of the NYNE test system with and without contribution of DVPP for scenario 3.

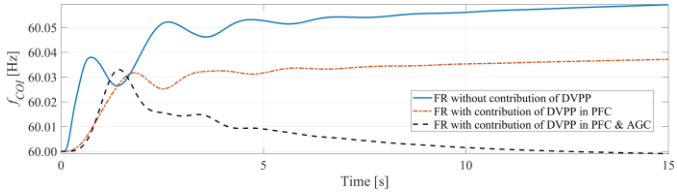

Fig. 11. Comparison of FR of the NYNE test system with and without contribution of DVPP for scenario 4.

Finally, the effectiveness of (35) and (36) in updating the reference signals in response to changes in the ACE signals is demonstrated in Table XI. It is assumed that for each scenario in Table VIII, the size of the power imbalance decreases by 10%. The results reported in Table XI, illustrating the variation of the reference signals consistent with the findings in Table VIII, closely align with the precise results obtained by following the same procedures as in (24)-(26).

To further justify the scalability of the proposed approach, let's consider a scenario where the NYNE test system incorporates 5 DVPPs, each tasked with delivering ancillary services to specific areas. The SO has mandated these DVPPs to collectively provide a maximum FRR capacity of 123.5 MW, with individual allocations of 25 MW, 25 MW, 20 MW, 35 MW, and 18.5 MW for each DVPP, respectively. Now, imagine a situation in which the SO calls upon these DVPPs to deliver 85 MW of FRR in response to a load being switched on in area 1. Table XII compares the results of the proposed method with those obtained using [15] where a Lyapunov function is integrated into the RL-based method to optimize the allocation of PFC among resources.

TABLE VII
COMPARISON OF ROCOF RELATED TO COI FOR THE PROPOSED METHOD AND [15]

Scenario	1	2	3	4
Proposed method	0.0571	0.0413	0.0531	0.0163
Ref. [15]	0.7619	0.0416	0.0531	0.1333
Without DVPP	0.8315	0.0423	0.0534	0.2114

TABLE VIII
PARAMETERS VARIATIONS

#	$\Delta(\Delta P_L)$	$\Delta p^{cluster_1}$	$\Delta p^{cluster_2}$	$\Delta p^{cluster_3}$	$\Delta p^{cluster_4}$	$\Delta p^{cluster_5}$
1	-10%	5%	6%	-4%	3%	2%
2	15%	-3%	8%	7%	6%	-7%
3	15%	-4%	-2%	4%	10%	7%
4	20%	-4%	9%	6%	-13%	11%

TABLE IX
NEW PFC SETPOINT SIGNALS IN RESPONSE TO CHANGING OF WEATHER CONDITION AND APPLIED FAULT

$\Delta P_{DVPP-ref}^{PFC_i}$	*Area 1*	*Area 2*	*Area 3*	*Area 4*	*Area 5*
1	0.23-0.04	0.11-0.07	0.20+0.15	0.08-0.03	0.38-0.01
2	0.18+0.06	0.18-0.09	0.24-0.11	0.10-0.05	0.30+0.19
3	0.06+0.17	0.45+0.06	0.23-0.10	0.15-0.09	0.11-0.04
4	0.22+0.08	0.13-0.04	0.31-0.18	0.16+0.18	0.18-0.04

TABLE X
ERROR BETWEEN THE RESULTS OF TABLE IX AND THE EXACT VALUES

$\Delta P_{DVPP-ref}^{PFC_i}$	*Area 1*	*Area 2*	*Area 3*	*Area 4*	*Area 5*
1	1.8%	0.65%	~0.00%	0.43%	0.3%
2	0.3%	0.42%	0.72%	0.81%	~0.00%
3	0.87%	0.13%	~0.00%	~0.00%	0.37%
4	0.12%	~0.00%	0.42%	~0.00%	~0.00%

TABLE XI
VARIATION OF THE REFERENCE SIGNALS IN RESPONSE TO CHANGES IN THE ACE SIGNAL

$\Delta P_{DVPP-ref}^{SFC_i}$	*Area 1*	*Area 2*	*Area 3*	*Area 4*	*Area 5*
Scenario 1	0.37	0.11	0.22	0.09	0.11
Scenario 2	0.17	0.36	0.19	0.06	0.12
Scenario 3	0.23	0.27	0.10	0.18	0.12
Scenario 4	-0.26	-0.16	-0.34	-0.23	-0.11

TABLE XII
COMPARISON OF FRR FOR THE PROPOSED METHOD AND [15] FOR 85 MW LOAD DISTURBANCE

DVPP	1	2	3	4	5
Proposed method	22.8	15.2	13.5	15	18.5
Ref. [15]	21.28	15.22	13	17	18.5

TABLE XIII
COMPARISON OF FRR FOR THE PROPOSED METHOD AND [15] FOR 88 MW LOAD DISTURBANCE

DVPP	1	2	3	4	5
Proposed method	23.6	15.6	14.2	15.3	19.3
Ref. [15]	9.71	24.61	7.41	27.77	18.5

Although both methods can meet the system's FRR requirement, the proposed approach achieves setpoint adjustments in a single try, while [15] requires three iterative attempts.

Let's consider a scenario where, in response to real-time weather changes affecting the operation of wind farms operating in grid-following mode, the SO updated the command reference signal to 88 MW. Table XIII presents a comparison between the outcomes achieved through the suggested approach and those derived from [15].

The outcomes presented in Table XIII demonstrate that minor fluctuations in the input data of the nonlinear RL-based controller from [15] have a noteworthy impact on the reference signal for each resource involved in PFC service. When collaborating with SGs for PFC, these substantial variations in IBRs result in unnecessary mechanical movements of SG governors, thereby diminishing their operational lifespan. On the contrary, the approach proposed in this paper effectively addresses algorithmic stability by utilizing Taylor expansion around the operating point, ensuring moderate variations in the reference signals in response to small variations in input data.

IV. CONCLUSION

This research contributes to the development of an effective and practical approach for online frequency regulation considering the contribution of IBRs, offering valuable insights for power system operation and control. The study examines RESs simultaneously at both the distribution and transmission levels. Without loss of generality, the RESs are aggregated into a unified entity known as the DVPP, which is treated from the SO's perspective as a participant in the frequency regulation service. The proposed mathematically

derived formulations aim to effectively allocate the FRR and AGC signals between the resources within the DVPP to restore the frequency to its nominal value. The results demonstrate that the proposed frameworks successfully regulate the frequency in real-time using PFC and SFC loops. Moreover, the study highlights the importance of designating one of the clusters as the slack cluster, which compensates for measurement errors and simplifications in the calculations.

While the TDS validates the allocation of resources to provide SFC, the internal dispatch of resources within DVPP should take into account the economics of resource dispatching. Furthermore, coordinating between DSOs and SOs is another area of interest for the successful integration of IBRs at the distribution level into regulatory services. These aspects should be further discussed in future works.

REFERENCES

[1] B. J. Kirby, "Frequency regulation basics and trends," U.S. Department of Energy, OAK Ridge National Laboratory, 2005.

[2] J. Björk, K. H. Johansson, and F. Dörfler, "Dynamic virtual power plant design for fast frequency reserves: Coordinating hydro and wind," *IEEE Transactions on Control of Network Systems*, 2022.

[3] H. Bevrani, T. Kato, T. Ise, and K. Inoue, *Grid Connected Converters: Modeling, Stability and Control*. Elsevier, 2022.

[4] A. Ademola-Idowu and B. Zhang, "Frequency stability using MPC-based inverter power control in low-inertia power systems," *IEEE Transactions on Power Systems*, vol. 36, no. 2, pp. 1628-1637, 2020.

[5] O. Stanojev, U. Markovic, P. Aristidou, G. Hug, D. Callaway, and E. Vrettos, "MPC-based fast frequency control of voltage source converters in low-inertia power systems," *IEEE Transactions on Power Systems*, vol. 37, no. 4, pp. 3209-3220, 2020.

[6] L. Kumar, S. Ahmed, R. Naidoo, and R. C. Bansal, "Decentralized reinforce-control of renewable dynamic virtual power plant enabling it to offer ancillary services: An attempt towards net-zero targets," *IET Renewable Power Generation*, 2022.

[7] V. Häberle, M. W. Fisher, E. Prieto-Araujo, and F. Dörfler, "Control design of dynamic virtual power plants: An adaptive divide-and-conquer approach," *IEEE Transactions on Power Systems*, vol. 37, no. 5, pp. 4040-4053, 2021.

[8] E. Dall'Anese, S. S. Guggilam, A. Simonetto, Y. C. Chen, and S. V. Dhople, "Optimal regulation of virtual power plants," *IEEE transactions on power systems*, vol. 33, no. 2, pp. 1868-1881, 2017.

[9] T. Anderson *et al.*, "Frequency regulation with heterogeneous energy resources: A realization using distributed control," *IEEE Transactions on Smart Grid*, vol. 12, no. 5, pp. 4126-4136, 2021.

[10] L. D. Espinosa, A. Khurram, and M. Almassalkhi, "Reference-tracking control policies for packetized coordination of heterogeneous DER populations," *IEEE Transactions on Control Systems Technology*, vol. 29, no. 6, pp. 2427-2443, 2020.

[11] N. Gu, J. Cui, and C. Wu, "An Auto-Tuned Robust Dispatch Strategy for Virtual Power Plants to Provide Multi-Stage Real-time Balancing Service," *IEEE Transactions on Smart Grid*, 2023.

[12] Z. Yan and Y. Xu, "Data-driven load frequency control for stochastic power systems: A deep reinforcement learning method with continuous action search," *IEEE Transactions on Power Systems*, vol. 34, no. 2, pp. 1653-1656, 2018.

[13] S. Sadeghi, H. Jahangir, B. Vatandoust, M. A. Golkar, A. Ahmadian, and A. Elkamel, "Optimal bidding strategy of a virtual power plant in day-ahead energy and frequency regulation markets: A deep learning-based approach," *International Journal of Electrical Power & Energy Systems*, vol. 127, p. 106646, 2021.

[14] Z. Yi *et al.*, "An Improved Two-Stage Deep Reinforcement Learning Approach for Regulation Service Disaggregation in a Virtual Power Plant," *IEEE Transactions on Smart Grid*, vol. 13, no. 4, pp. 2844-2858, 2022.

[15] W. Cui, Y. Jiang, and B. Zhang, "Reinforcement learning for optimal primary frequency control: A Lyapunov approach," *IEEE Transactions on Power Systems*, vol. 38, no. 2, pp. 1676-1688, 2022.

[16] M. Polycarpou, J. Farrell, and M. Sharma, "On-line approximation control of uncertain nonlinear systems: issues with control input saturation," in *Proceedings of the 2003 American Control Conference, 2003.*, 2003, vol. 1: IEEE, pp. 543-548.

[17] D. E. Ochoa, F. Galarza-Jimenez, F. Wilches-Bernal, D. Schoenwald, and J. I. Poveda, "Control Systems for Low-Inertia Power Grids: A Survey on Virtual Power Plants," *IEEE Access*, 2023.

[18] K. Yan, G. Li, R. Zhang, Y. Xu, T. Jiang, and X. Li, "Frequency Control and Optimal Operation of Low-Inertia Power Systems with HVDC and Renewable Energy: A Review," *IEEE Transactions on Power Systems*, 2023.

[19] B. Marinescu. "POSYTYF concept and objectives." https://posytyf-h2020.eu/project-overview/project-structure (accessed 2023).

[20] B. Marinescu, O. Gomis-Bellmunt, F. Dörfler, H. Schulte, and L. Sigrist, "Dynamic virtual power plant: A new concept for grid integration of renewable energy sources," *IEEE Access*, vol. 10, pp. 104980-104995, 2022.

[21] R. H. Lasseter, Z. Chen, and D. Pattabiraman, "Grid-forming inverters: A critical asset for the power grid," *IEEE Journal of Emerging and Selected Topics in Power Electronics*, vol. 8, no. 2, pp. 925-935, 2019.

[22] B. B. Johnson, S. V. Dhople, A. O. Hamadeh, and P. T. Krein, "Synchronization of parallel single-phase inverters with virtual oscillator control," *IEEE Transactions on Power Electronics*, vol. 29, no. 11, pp. 6124-6138, 2013.

[23] E. O. Kontis, Á. R. del Nozal, J. M. Mauricio, and C. S. Demoulias, "Provision of primary frequency response as ancillary service from active distribution networks to the transmission system," *IEEE Transactions on Smart Grid*, vol. 12, no. 6, pp. 4971-4982, 2021.

[24] M. E. Adabi and B. Marinescu, "Direct Participation of Dynamic Virtual Power Plants in Secondary Frequency Control," *Energies*, vol. 15, no. 8, p. 2775, 2022.

[25] S. Ghosh and M. El Moursi, "An Analytical Approach for Frequency Estimation of Modern Power Grid," *IEEE Transactions on Power Systems*, vol. 37, no. 5, pp. 4094-4097, 2022.

[26] F. Milano and A. Ortega, "Frequency divider," *IEEE Transactions on Power Systems*, vol. 32, no. 2, pp. 1493-1501, 2016.

[27] H. Golpîra and A. R. Messina, "A center-of-gravity-based approach to estimate slow power and frequency variations," *IEEE Transactions on Power Systems*, vol. 33, no. 1, pp. 1026-1035, 2017.

[28] H. Golpîra, A. Román-Messina, and H. Bevrani, *Renewable Integrated Power System Stability and Control*. John Wiley & Sons, 2021.

[29] H. Golpîra, A. R. Messina, and H. Bevrani, "Emulation of virtual inertia to accommodate higher penetration levels of distributed generation in power grids," *IEEE Transactions on Power Systems*, vol. 34, no. 5, pp. 3384-3394, 2019.

[30] G. C. Kryonidis *et al.*, "Use of ultracapacitor for provision of inertial response in virtual synchronous generator: Design and experimental validation," *Electric Power Systems Research*, vol. 223, p. 109607, 2023.

[31] H. Bevrani, *Robust power system frequency control*. Springer, 2014.

[32] "Balancing and Frequency Control Reference Document," NERC Resources Subcommittee, 2021.

[33] K. Oureilidis *et al.*, "Ancillary services market design in distribution networks: Review and identification of barriers," *Energies*, vol. 13, no. 4, p. 917, 2020.

[34] P. S. Kundur and O. P. Malik, *Power system stability and control*. McGraw-Hill Education, 2022.

[35] X. Zhang *et al.*, "Deloading power coordinated distribution method for frequency regulation by wind farms considering wind speed differences," *IEEE Access*, vol. 7, pp. 122573-122582, 2019.

[36] H. Golpîra, H. Bevrani, A. R. Messina, and B. Francois, "A data-driven under frequency load shedding scheme in power systems," *IEEE Transactions on Power Systems*, vol. 38, no. 2, pp. 1138-1150, 2023.

[37] G. Rogers, *Power system oscillations*. Springer Science & Business Media, 2012.